Research Article

Žiga Jelen, Marcin Krajewski, Franc Zupanič, Peter Majerič, Tilen Švarc, Ivan Anžel, Jernej Ekar, Sz-Chian Liou, Jerzy Kubacki, Mateusz Tokarczyk, and Rebeka Rudolf*

# Melting point of dried gold nanoparticles prepared with ultrasonic spray pyrolysis and lyophilisation

https://doi.org/10.1515/ntrev-2022-0568
received April 7, 2023; accepted June 12, 2023

**Abstract:** A coupled process of ultrasonic spray pyrolysis and lyophilisation was used for the synthesis of dried gold nanoparticles. Two methods were applied for determining their melting temperature: uniaxial microcompression and differential scanning calorimetry (DSC) analysis. Uniaxial microcompression resulted in sintering of the dried gold nanoparticles at room temperature with an activation energy of 26–32.5 J/g, which made it impossible to evaluate their melting point. Using DSC, the melting point of the dried gold nanoparticles was measured to be around 1064.3°C, which is close to pure gold. The reason for the absence of a melting point depression in dried gold nanoparticles was their exothermic sintering between 712 and 908.1°C.

**Keywords:** gold nanoparticles, melting point, ultrasonic spray pyrolysis, characterisation

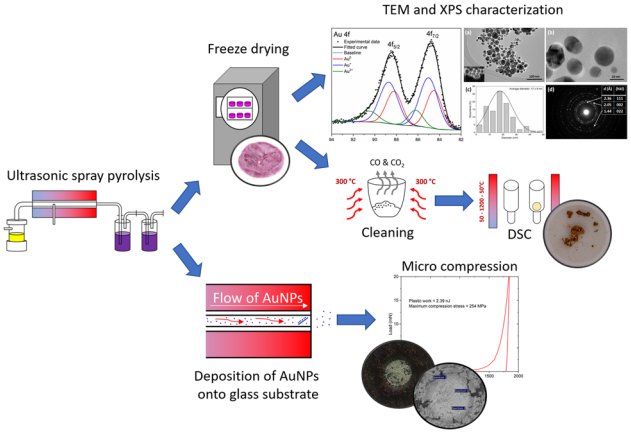


**Graphical abstract**

## Abbreviations

| | |
|---|---|
| AuNPs | gold nanoparticles |
| DSC | differential scanning calorimetry |
| EDS | energy-dispersive spectroscopy |
| FIB | focused ion beam |
| HRTEM | high-resolution transmission electron microscopy |
| PVP | polyvinylpyrrolidone |
| SAED | selected area electron diffraction |
| SEM | scanning electron microscope |
| TEM | transmission electron microscope |
| USP | ultrasonic spray pyrolysis |
| XPS | X-ray photoelectron spectroscopy |
| XRD | powder X-ray diffraction |

## 1 Introduction

Gold nanoparticles (AuNPs) are extremely interesting, because they have completely different electronic, optical, and thermal properties compared to their bulk counterparts [1]. All the listed properties of AuNPs are exactly adjustable by the design

* **Corresponding author: Rebeka Rudolf**, Faculty of Mechanical Engineering, University of Maribor, Maribor, Slovenia; Zlatarna Celje d.o.o., Celje, Slovenia, e-mail: rebeka.rudolf@um.si
**Žiga Jelen, Franc Zupanič, Tilen Švarc, Ivan Anžel:** Faculty of Mechanical Engineering, University of Maribor, Maribor, Slovenia
**Marcin Krajewski:** Department of Mechanics of Materials, Institute of Fundamental Technological Research, Polish Academy of Sciences, Pawińskiego 5B, 02-106, Warsaw, Poland
**Peter Majerič:** Faculty of Mechanical Engineering, University of Maribor, Maribor, Slovenia; Zlatarna Celje d.o.o., Celje, Slovenia
**Jernej Ekar:** Department of Surface Engineering and Optoelectronics, Institut Jožef Stefan, Jamova 39, SI-1000, Ljubljana, Slovenia
**Sz-Chian Liou:** Electron Microscopy Facility, Institute for Functional Materials and Devices, Lehigh University, Bethle-hem, PA 18015, USA
**Jerzy Kubacki:** Faculty of Science and Technology, Institute of Physics, University of Silesia in Katowice, 75 Pułku Piechoty 1, 41-500 Chorzów, Poland
**Mateusz Tokarczyk:** Faculty of Physics, Institute of Experimental Physics, University of Warsaw, Pasteura 5, 02-093 Warsaw, Poland

and modification of selected types of synthesis (Turkevich method, Brust–Schriffrin method, laser ablation, seed growth, ultrasonic spray pyrolysis [USP]) [2–5] and their parameters [6]. Recently, a variety of different methods for reproducible and well-known synthesis of nanoscale AuNPs were developed [2,7–9]. High-throughput industrial methods [9–11] generally fall into this category, as they synthesise nanoparticles with a very narrow size distribution and shape.

USP is a method that allows for an adequate degree of size control and a relatively high production capacity of different solid nanoparticles, whereby their collection is possible either in electromagnetic filters, or in collection systems with different suspensions. Various stabilisers and modifiers can be added to suspensions, depending on the type of nanoparticles and their use.

Nowadays, there is an increasing demand for dried nanoparticles. Due to the written requirement, attempts are being made to synthesise AuNPs using a combination of different methods, since there is practically no process that would allow reaching the dried state in one step. Recently, a coupled process using USP and lyophilisation has been developed, where the end products are dried AuNPs [10]. Lyophilisation has been known as an established drying technology, which has already been transferred to an industrial level in the food and pharmaceutical industries. The lyophilisation drying process takes place at a cryogenic temperature and an extremely low pressure, which enables the preservation of the final properties of the dried material achieved by previous synthesis processes [12].

Most bulk materials have well-defined, or even standardised melting points, the value of which does not depend on their size. However, as the size of the material decreases towards the nanometre size and approaches the atomic scale, the dependence increases strongly with the dimensions of the material. Nanoparticles do not have the same properties as bulk materials, as their melting points are tens, if not hundreds, of degrees lower than their bulk counterparts. This phenomenon, called melting-point depression, was first confirmed experimentally, as the lower melting temperatures of metal thin film surfaces from 1 to 100 nm were measured by observing the change in diffraction pattern in correspondence to temperature [13]. Since then, many experimental methods have been proposed to determine the melting point of nanoparticles, such as using the beam of an electron microscope to induce heating and nano calorimeters [14]. In parallel, several mathematical models have been postulated that describe the possible mechanisms of nanoparticle melting [15,16]. Although experimental techniques, such as transmission electron microscopy (TEM) observation, nanocalorimetry, and X-ray diffraction, have been established to study the melting process of nanoparticles, the understanding of this problem has not been addressed satisfactorily, because it is not applicable to measure the temperature of a free-standing, mass-selected nanoparticle in a vacuum.

The fact that nanoparticles have a melting point depression has opened up the possibilities of their new uses for the purposes of producing catalysts, semiconductors, sensors, *etc.* [17,18]. Conductive nanoparticles with a melting point depression have potential for use in smart devices [19–22], that can be implanted into the human body noninvasively. These devices are usually manufactured using different printing and filtering methods, so that the formulation of suitable inks is a major challenge (compatibility with flexible substrates such as polyethylene terephthalate, PET; heat treatment at $T < 150$°C, conductivity, *etc.*). Dried AuNPs certainly belong to this promising group for the preparation of inks, which stand out for their properties, among which is electrical conductivity ($\sigma = 4.42 \times 10^7\ \Omega^{-1}\ m^{-1}$) [23].

In the preparation of ink, the process of oxidation of nanoparticles is crucial. The use of nanoparticles, which are highly conductive but prone to oxidation, leads to the formation of a thicker oxide layer, which usually requires a higher temperature during the subsequent heat treatment of the printed layer and results in lower electrical conductivity [24,25]. Since bulk gold is a noble metal and chemically inert, as it does not form a thick oxide layer on its surface, AuNPs are also characterised by high chemical stability. This makes them the most promising candidates for the preparation of nanoparticle inks. For the practical use of dried AuNPs, it is necessary to know the melting point temperature, as the basic processing processes, such as heat treatment, sintering, annealing, *etc.*, depend on it.

Based on the presentation of the scientific problem, the aim of this research was to determine the melting temperature of dried AuNPs, which were synthesised by a combination of coupled USP and lyophilisation methods. Various characterisation techniques (differential scanning calorimetry [DSC], energy-dispersive spectroscopy [EDS], focused ion beam [FIB], high-resolution transmission electron microscopy [HRTEM], scanning electron microscopy (SEM), TEM, X-ray photoelectron spectroscopy [XPS], and X-ray diffraction [XRD]) were used for this purpose, and a melting point comparison was made with pure Au ($T = 1064.2$°C) [26]. It was hypothesised that the measured value of the melting temperature will enable the determination of other related properties of AuNPs indirectly, so that, in the future, they could be carried out in a controlled manner into various new applications.

# 2 Materials and methods

## 2.1 USP Synthesis of AuNPs

AuNPs were synthesised using a custom USP device (Zlatarna Celje, d.o.o.) [27] that utilises a 1.65 MHz piezo transducer to aerosolise a precursor of 1.0 g/l aqueous solution of gold chloride (hydrogen tetrachloroaurate(III) trihydrate, $HAuCl_4$, Glentham Life Sciences, UK). The generated aerosol is fed with $N_2$ gas into a quartz reaction tube heated to 400°C, where $H_2$ is introduced to facilitate reduction of the gold salt into AuNPs. The AuNPs were collected in an aqueous solution of polyvinylpyrrolidone (PVP; average MW 40,000; Sigma-Aldrich, China) with a concentration of 2.5 g/l PVP. The PVP acts as bots, a steric stabiliser, and cryo protectant [28,29], which was key for the next step of freeze-drying. Before freeze-drying, the produced AuNPs' suspension was concentrated by rotary evaporation using a Büchi Rotavapor R-300 (Büchi Labortechnik AG, Flawil, Switzerland), at a vapour pressure of 25 mPa, 195 rpm rotation speed, and bath temperature of 35°C. The obtained suspension was then further concentrated with a centrifuge Centurion C2000 (Centurion Scientific Limited, Chichester, UK), at 10,000 rpm, using a PTFE 100,000 MWCO membrane (0.1 µm pore size) for filtration. The final concentration of Au in the AuNPs' suspension was 5.5 mg/ml, measured by ICP-OES (Agilent 5800 VDV, CA, USA),

## 2.2 Lyophilisation of AuNPs

The freeze-drying was performed on Labfreez instruments FD-200F SERIES (Labfreez Instruments Group Co., Ltd, Beijing, China), over the course of 49 h (2 days). The freeze-drying parameters were set as shown in Table 1.

Upon lyophilisation, the resulting dried AuNPs were entrapped in a cake of PVP stabiliser as shown in Figure 1.

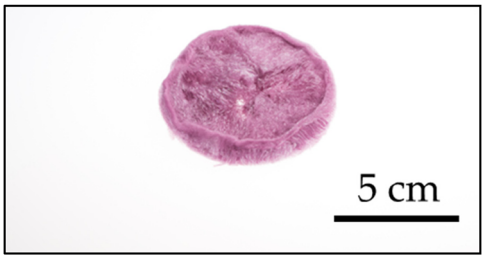


**Figure 1:** Macro view of dried AuNPs after lyophilisation.

## 2.3 Characterisation of the dried AuNPs

The morphology and crystal structure of the dried AuNPs were investigated by means of a JEOL 2100 FEG (scanning) transmission electron microscope ((S)TEM) equipped with a Bruker XFlash EDS detector. The TEM investigations were carried out at 200 kV of accelerating voltage. The dried AuNPs were suspended in absolute anhydrous ethanol and mixed in an ultrasonic bath for 5 min. Then, a few drops of the suspension were pipetted onto a TEM grid coated with holey carbon films (Ted Pella Inc.) and air-dried. Moreover, the collected TEM images of the AuNPs were used to determine their size distribution with the ImageJ software [30]. The distribution diagram was calculated for the collection of 100 measured AuNPs. The obtained histogram was fitted to a log-normal distribution, which was then used to estimate the average diameter of single AuNPs.

A powder XRD measurement of the dried AuNPs was performed using a Phillips X'Pert diffractometer equipped with a Cu-sealed tube (X-ray source, $\lambda$ = 0.1542 nm) and a parallel beam Bragg reflection mirror. The data were collected with a step of 0.1° and a collecting time of 15 s per each step.

The surface chemical composition of the dried AuNPs was determined using XPS. The measurements were carried out with a PHI 5700/660 Physical Electronics spectrometer equipped with an Al anode providing a monochromatic X-ray source with an energy of 1486.6 eV. The energy resolution in the XPS measurements did not exceed 0.35 eV, whereas the X-ray radiation spot on the sample was about 1 mm in diameter. The sample was placed on a standard PREVAC sample holder with the use of carbon tape. The XPS device was calibrated according to the peak positions of Au $4f_{7/2}$ at 83.98 eV, Ag $3d_{5/2}$ at 368.27 eV, and Cu $2p_{3/2}$ at 932.67 eV. The chemical composition was conducted on the obtained data with MultiPak software provided by Physical Electronics.

**Table 1:** Freeze-drying parameters

| Stage | Temperature (°C) | Time (h) | Pressure (Pa) |
|---|---|---|---|
| Freezing | −40 | 4 | Ambient |
| Primary drying | +20 | 12 | 1–4 |
| Secondary drying | +30 | 33 | 1–4 |

## 2.4 AuNPs' microcompression

### 2.4.1 Preparation of an AuNPs' sample

To carry out microcompression measurements, it was necessary to prepare a suitable sample with AuNPs, so

that the influence of any other process on the change of AuNPs in terms of their size, morphology, chemical composition, or final properties was minimal. Based on this, a borosilicate glass target of size 20 mm × 20 mm with a thickness of 1 mm was selected, which was placed at an angle of 45° at the outlet of the reaction zone in the USP devices. This enabled the direct collection of the synthesised bare and unestablished AuNPs on the surface of the target. The USP synthesis took place for 1 h under the same conditions as described in point 2.1. A layer of AuNPs with a thickness of 1–2 µm was formed on the target.

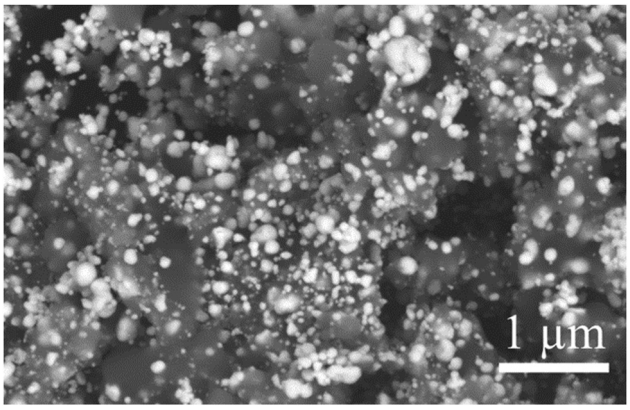


**Figure 2:** SEM micro view of AuNPs after oxidation of the PVP (AuNPs on carbon film).

#### 2.4.2 Measurement

Microcompression measurements were performed with NanoTest Vantage (MML) directly on AuNPs collected on a borosilicate glass target without any additional preparation. A flat imprint head in the shape of a circle with a diameter of 10 µm was used for all measurements.

Optical images of the indentation sites were performed with a Keyence VHX-7000 Digital Microscope (Keyence, Japan).

A Sirion 400 NC SEM (FEI, Hillsboro, OR, USA), equipped with an INCA 350 EDS detector (Oxford Instruments, Abingdon, Oxfordshire, UK), was used for observation of the microstructure and determination of the chemical composition of the indentation sites. The FIB method with a gallium liquid metal ion source on an environmental Scanning Electron Microscope Quanta 3D (FEI) was used for the preparation of a cross-section, to gain insight into the microstructure and chemical composition beneath the impression surface.

### 2.5 Determination of the melting temperature for AuNPs

#### 2.5.1 Preparation of an AuNPs' sample

The dried AuNPs were treated further by oxidation at 400°C in air to remove the residual PVP from the cake. The heat-treated AuNPs retained their characteristic "red" colour and did not agglomerate or sinter. Their SEM micro view is shown in Figure 2.

#### 2.5.2 DSC analysis

The melting temperature of AuNPs was measured experimentally using a DSC method. The high-temperature DSC data were collected with a Mettler Toledo TGA/DSC 3+ (Mettler Toledo, Switzerland) thermal analyser, with a TGA-DTA Sensor LF/HT. The measurements were performed in an $N_2$ atmosphere with a flow rate of 50 ml/min. Heating was performed from 25 to 1,200°C, with a heating rate of 10°C/min; the sample was kept at 1,200°C for 2 min.

## 3 Results and discussion

### 3.1 TEM

The results of the TEM investigations of the dried AuNPs are collected in Figure 3. Figure 3a and b presents the HRTEM images. Analysing them, one can see that the investigated AuNPs seem to be composed only of a gold phase. Moreover, the AuNPs are mostly separated from each other. This confirms that stabilisation and freeze-drying reduce their tendency to form the agglomerations. The scanning TEM-EDS mapping indicates that the AuNPs are covered by a thin carbon layer, which confirms the presence of the PVP stabiliser on the surface of the AuNPs. Based on the recorded images, the particle size distribution diagram of the AuNPs was determined and is shown in Figure 3c. The spread of their diameters ranges between 4 and 47 nm, but their average size is about 17 nm. The variation in size is a direct consequence of the method of aerosolisation used with USP, which produces a mist of fine droplets that are mainly around 3 µm in diameter, with a number of them being smaller or larger [31]. The selected area electron diffraction (SAED) pattern has also been collected for the AuNPs in parallel to the TEM measurements and is presented in Figure 3d. The obtained pattern consists of five rings. Such a pattern is typically obtained for the polycrystalline materials [32]. This indicates that the

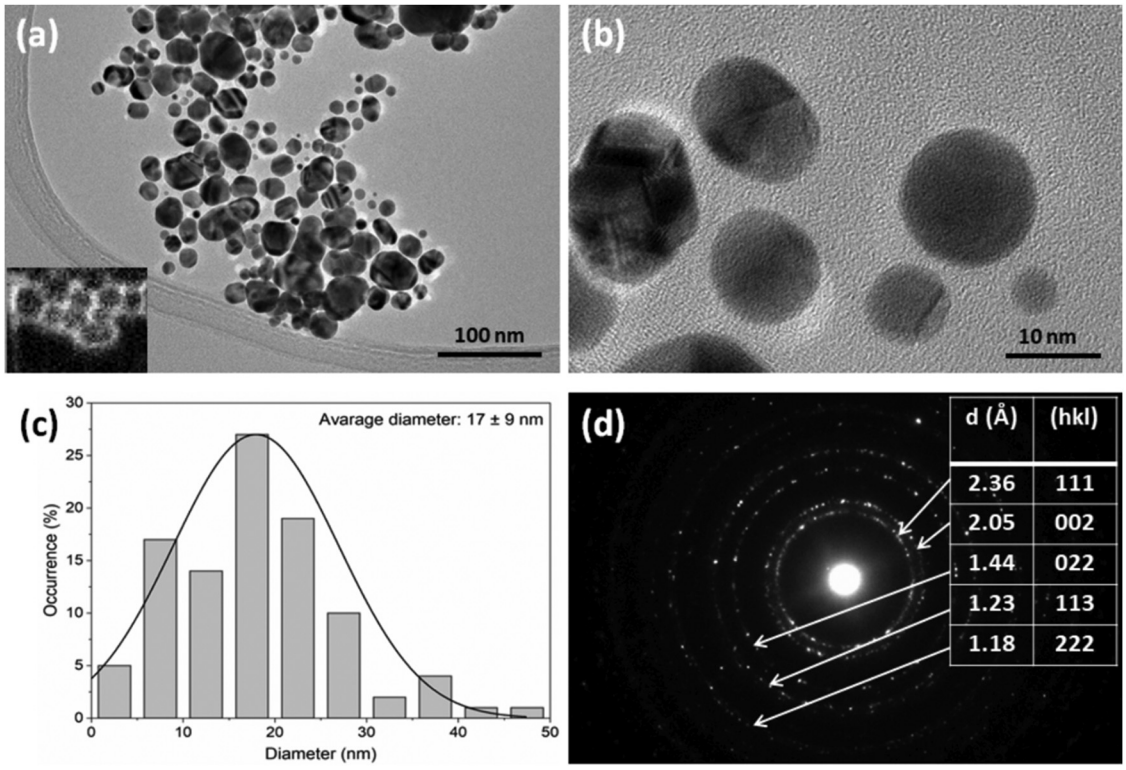


**Figure 3:** HRTEM images of AuNPs with (a) low magnification (inset – carbon elemental mapping performed with STEM-EDS) and (b) high magnification. (c) Particle size distribution diagram of AuNPs. (d) SAED pattern of AuNPs recorded for Figure 2a.

larger AuNPs are composed of several grains (cf. Figure 3b), which are formed due to the non-uniform diffusion process of [Au] during the USP synthesis. The rings of the SAED pattern refer to the (111), (200), (220), (311), and (222) crystal planes, and the corresponding estimated interplanar distances equal 2.36, 2.05, 1.44, 1.23, and 1.18 Å, respectively. No additional rings coming from the other phases are observed; thus, the AuNPs seem to be highly pure single phase.

## 3.2 UV-Vis

UV-Vis absorption spectroscopy was used to characterise the optical properties of the aqueous suspension of AuNPs, which was prepared by dissolving the dried AuNPs in demineralised water, to achieve an approximate concentration of 100 ppm (Au). The measurements were performed using a Tecan Infinite M200 (Tecan Group Ltd., Männedorf, Switzerland), using a special microplate with the following parameters: sample volume: 300 µL, absorbance range: $\lambda$ = 300–800 nm, no., flashes: 5×. The peak absorbance was measured at 532 nm, as shown in Figure 4. This is in agreement with our previous observations [10]. The single slightly elongated peak indicates a degree of size dispersity that was also observed with TEM, and a high degree of size conformity, with the majority of the AuNPs being circular. The Surface Plasmon Resonance of the measured AuNPs causes increased absorption of visible light, with wavelengths around the absorption peak and below the peak. As seen from the graph in Figure 4, the visible light becomes absorbed more strongly at wavelengths below about 600 nm. From the visible light colour spectrum, this corresponds to green, blue, and violet light, at wavelengths 550, 450, and 400 nm, along with some yellow colour being absorbed as well at wavelengths of around 600 nm. The

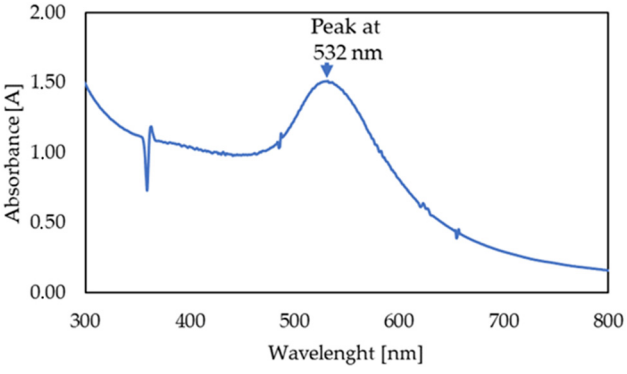


**Figure 4:** UV-Vis spectra of aqueous suspension of redispersed AuNPs.

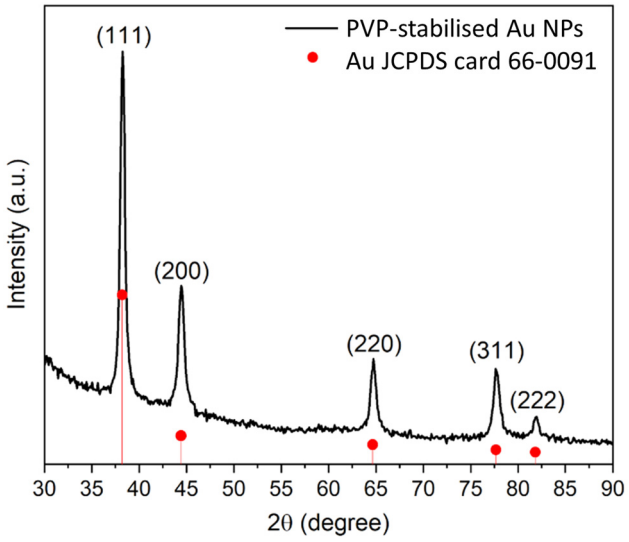


**Figure 5:** XRD pattern of the AuNPs; the positions of diffraction peaks; and corresponding Miller indices are assigned according to the JCPDS card no. 66-0091.

visible light above the peak absorption value, corresponding to the red colour at wavelengths of around 700 nm, is being absorbed less according to the absorbance spectrum. The resulting absorption effect is visible from the aqueous suspensions of the measured AuNPs, which have a bright red colour.

## 3.3 XRD

The XRD pattern collected for the AuNPs is shown in Figure 5. The recorded pattern consists of five quite sharp diffraction peaks, whose angle positions fit well to the Au phase. The

**Table 2:** Atomic and weight content of elements forming the AuNPs determined from the XPS measurements

| C 1s | N 1s | O 1s | Cl 2p | Au 4f | Sum |
|---|---|---|---|---|---|
| | | **Atomic content (%)** | | | |
| 92.56 | 5.02 | 1.58 | 0.65 | 0.19 | 100.00 |
| | | **Weight content (%)** | | | |
| 87.66 | 5.54 | 2.00 | 1.81 | 2.99 | 100.00 |

Miller indices are assigned according to the JCPDS card no. 66-0091. Considering the XRD data, the value of crystalline size estimated from the Scherrer equation is 12.6 ± 1.0 nm. This value is comparable with the average diameter of the AuNPs based on the HRTEM images.

## 3.4 XPS

The results of XPS analysis performed for the dried AuNPs are collected in Figure 6a and Table 2. Analysing them, it is possible to notice that, apart from the Au XPS lines, the other lines referred to carbon, oxygen, nitrogen, chlorine, and titanium, which occurred in the XPS survey spectrum. The titanium signal and a part of the nitrogen signal come from the holder, which, in fact, had not been covered completely before the XPS measurement. The weak Cl 2p XPS line may have been detected due to incomplete reduction of the gold salt taken to the USP process. In turn, the origin of the carbon, nitrogen, and oxygen XPS lines is associated with that of the PVP stabiliser. This observation is in accordance with the EDS elemental mapping (cf. Figure 3). The atomic and weight content of the chemical elements forming the AuNPs are determined from the XPS survey

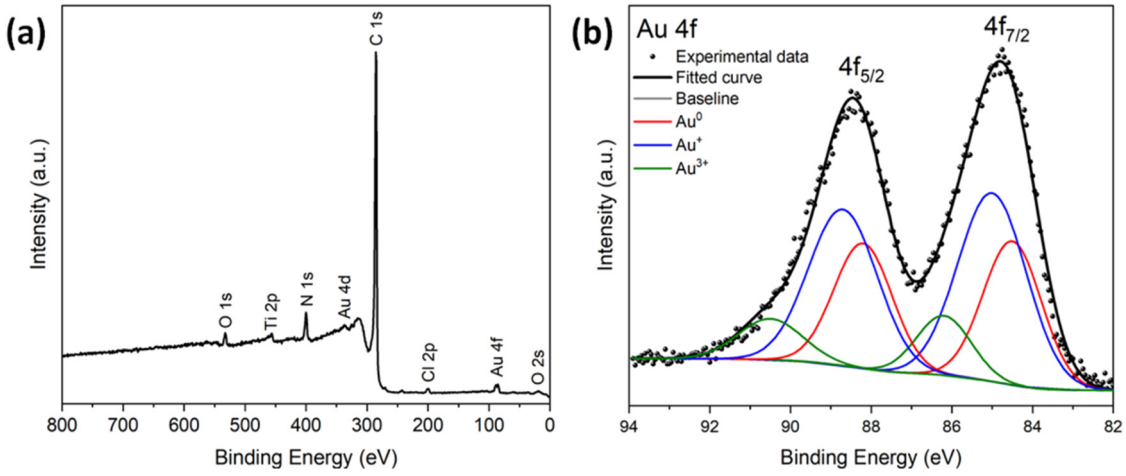


**Figure 6:** (a) Survey XPS spectrum of the dried AuNPs. (b) Au 4f XPS spectrum recorded for the AuNPs.

spectrum and are provided in Table 2. Comparing the obtained results and taking into account that the XPS method probes mostly the surface of the sample, it is clear that the AuNPs are covered by the PVP stabiliser.

The high-resolution Au 4f XPS spectrum is shown in Figure 6b. It consists of two well-defined Au $4f_{7/2}$ and Au $4f_{5/2}$ core lines corresponding to their spin–orbit coupling [33–35]. In addition, each of them can be deconvoluted into three components. It is worth noting that the binding energies (BE) of components forming the Au $4f_{7/2}$ band refer to the BE of components forming the Au $4f_{5/2}$ line. The distance between corresponding peaks is about 3.7 eV, and this observation is consistent with previously reported values [35–39]. The Au $4f_{7/2}$ line is formed of the components at the BE of 84.5, 85.1, and 86.2 eV, whereas the components located at 88.2, 88.7, and 90.4 eV are found for the Au $4f_{5/2}$ band. Considering only the position of the Au $4f_{7/2}$ line, which is used frequently for the calibration of XPS spectrometers [39], the measured BE values occur for $Au^0$ (84.5; FWHM 1.7), $Au^+$ (85.1; FWHM 2), and $Au^{3+}$ (86.2; FWHM 1.6) [34,35,39,40]. The presence of an $Au^{3+}$ ion in the sample can be explained by the incomplete reduction of the gold precursor ($HAuCl_4$) from the USP process. It is also known that the reduction of $HAuCl_4$ frequently passes through the intermediate steps in which the formation of $Au^+$-containing compounds occurs [38,40,41]. Therefore, it is possible that the $Au^+$ has been formed during the stabilisation process, to facilitate the binding between the PVP stabiliser and the AuNPs.

## 3.5 Microcompression

Figure 7 shows a load–depth diagram for the AuNPs. The thickness of the collected AuNPs was 1–2 µm. As the flat indentor touched the deposit it started to densify it. The load initially increased very slowly, since most of the particles were pushed away. The considerable increase occurred when the thickness of the layer was reduced to about 300 nm. After that, the densification occurred by plastic deformation of the AuNPs, and their spherical shape started to turn to the pancake one. The initial density of dislocations in nanoparticles is rather low [42], and the dislocation path is rather low; thus, the initial stress to cause the plastic deformation is very high. It is expected that dislocations were formed inside a single particle, and their density increased with deformation. A detailed model of nanoparticle deformation was given by Mayer [43]. At smaller compressing stresses, roughly below 250 MPa, the colour of the compacted AuNPs did not change, but at stresses above this value, the colour of the deposit at the compression site turned to a typical gold colour (Figure 8).

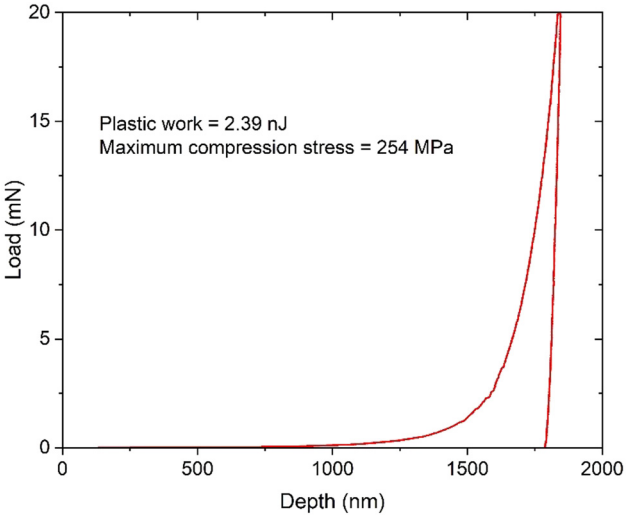


**Figure 7:** A typical load–depth diagram for a microcompression test of AuNPs on a borosilicate substrate.

The plastic work at the turning point was determined between 2.0–2.5 nJ. This value corresponds to 5,100–6,400 J/mol, or 26–32,5 J/g, which represents 40–50% of gold fusion heat. This energy can be treated as an activation energy for the room temperature sintering, which was also observed in other nanoparticles [44–47]. The stress can cause reorientation and coalescence of particles, which are enhanced by the formation of new, completely clean surfaces induced by plastic deformation. The observation opens new ways of producing bulk golden thin films from AuNPs at room temperature.

Optical microscopy showed that the imprint revealed a gold colour, while the edge of the imprint and the rest of the AuNPs test surfaces are red (Figure 8).

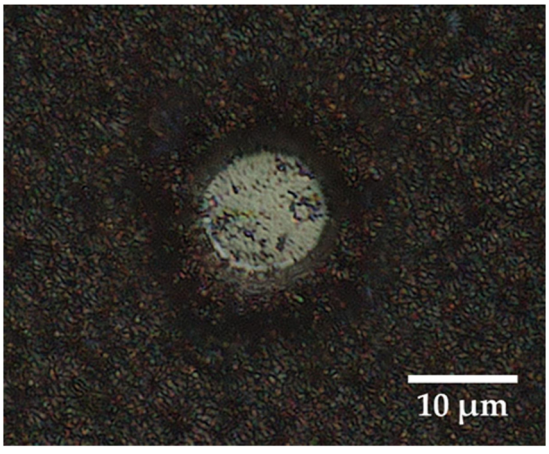


**Figure 8:** Optical micrograph of a microcompression site, with the visible area of imprinted AuNPs, which obtained a gold colour.

## 3.6 SEM

A detailed SEM examination of the AuNPs' surface, where the hardness measurement was performed by microcompression, revealed that the cold mutual pressing of AuNPs took place, which resulted in the formation of a bigger microparticle, as seen in Figure 9a. The results of the EDS analysis indicate a 100 wt% Au content without the presence of any impurities.

In the second stage, an FIB cut of the resulting microparticle was performed (Figure 9b), which removed practically half of the microparticle. The results of EDS analysis on the FIB cross-section showed an identical Au content (100 wt%) as on the whole surface of this microparticle. FIB cutting in metals and alloys allows the detection of the microstructure without any metallographic preparation. The exposed FIB section shows a microstructure that has the characteristics of pressed materials, with the presence of porosity in a smaller proportion by volume and in a larger proportion by the circumference of the microparticle.

In the case of microcompression, due to the transfer of energy to the surface of the AuNPs, which were located below the indenter surface, this caused their movement inside, and, thus, direct indentation into the AuNPs, which were within the volume of the test coating. This was followed by processes such as migration, rotation, coalescence, necking, and reshaping of the AuNPs, which caused their room-temperature sintering. A similar case is known from the interaction of the electron beam with AuNPs [48], where, due to the energy transfer, uniformly distributed AuNPs begin to migrate, rotate, coalesce, and aggregate, by ripening, necking, and reshaping to form larger AuNPs [49]. As a result of what has been presented, we can conclude that the additional external energy in the crystal structure of the AuNPs caused first the self-organisation of gold atoms and later the mutual imprinting of AuNPs, which resulted in a change in the colour of the AuNPs to gold.

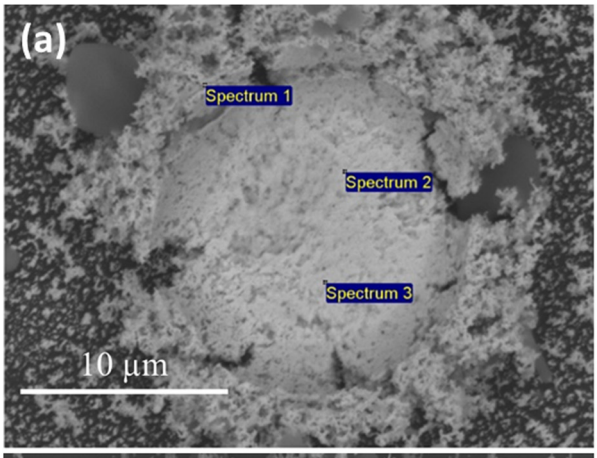


| Spectrum | In stats. | Au | Total |
|---|---|---|---|
| Spectrum 1 | Yes | 100.00 | 100.00 |
| Spectrum 2 | Yes | 100.00 | 100.00 |
| Spectrum 3 | Yes | 100.00 | 100.00 |
| Mean | | 100.00 | 100.00 |
| Std. deviation | | 0.00 | |
| Max. | | 100.00 | |
| Min. | | 100.00 | |

| Spectrum | In stats. | Au | Total |
|---|---|---|---|
| Spectrum 1 | Yes | 100.00 | 100.00 |
| Spectrum 2 | Yes | 100.00 | 100.00 |
| Spectrum 3 | Yes | 100.00 | 100.00 |
| Mean | | 100.00 | 100.00 |
| Std. deviation | | 0.00 | |
| Max. | | 100.00 | |
| Min. | | 100.00 | |

**Figure 9:** SEM micrographs of areas where the microcompression of AuNPs was performed with corresponding EDS analysis: (a) directly on the surface after microcompression and (b) after FIB cross-section milling.

## 3.7 DSC

The DSC results indicated that AuNPs undergo an exothermic process (+1554.33 J/g) with an average initiation temperature of 712°C (Figure 10). This can most likely be attributed to a combination of (i) exothermic sintering caused by the reaction enthalpy of AuNPs, reducing their surface area *via* the sintering mechanism of grain boundary diffusion and surface diffusion [50–54], which causes a reduction in specific surface area and an increase in volume; (ii) the latter causes a reduction in the specific heat capacity of the AuNPs as they coalesce into porous bulk gold, and their individual volume increases [55,56]. The initial burst of energy subsides and is followed by a sharp decrease in specific heat capacity evident by the curve drop-off starting at an average of 908.12°C and followed by a close-to-normal melting temperature of gold. The curve drop indicates that all sintering processes have been completed, resulting in a residue of bulk gold, proven by an average melting point of 1064.32°C (very close to the theoretical 1064.18°C [26] melting point of bulk gold). The slight difference in melting point might be a consequence of device accuracy and calibration errors in such a wide temperature range.

A macroscopic examination of the AuNPs' sample after performing DSC analysis revealed that it had a golden colour, as shown in Figure 11.

The measured melting point for dried AuNPs synthesised by USP and lyophilisation (Figure 1) does not show compliance with the phenomenon called melting-point depression, which is known from the literature and applies

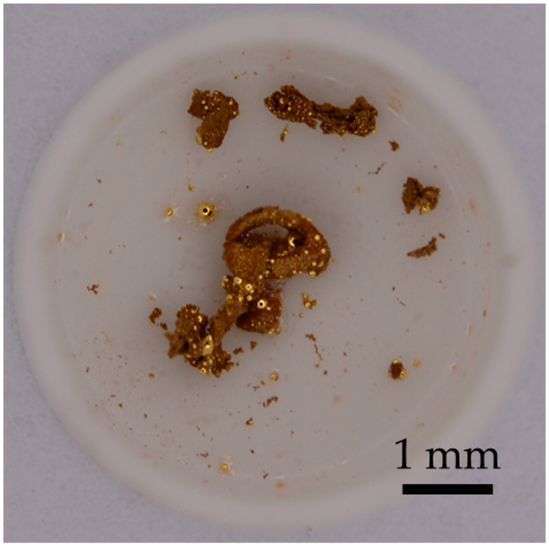


**Figure 11:** DSC sample cup after measurement with visible bulk Au.

in general to nanomaterials [10]. By TEM, XRD, and XPS characterisation, it was confirmed that the tested AuNPs can be classified as nanomaterials, both in terms of size distribution and average size and in terms of structure. On the contrary, the results of DSC analysis revealed the presence of a new phenomenon: exothermic sintering of AuNPs, which took place at a temperature lower than the melting point. This was likely due to the dried cake structure of the AuNPs, which is ultimately reflected in their comparable melting point to bulk Au. Further comparison with the existing literature and experimentally measured

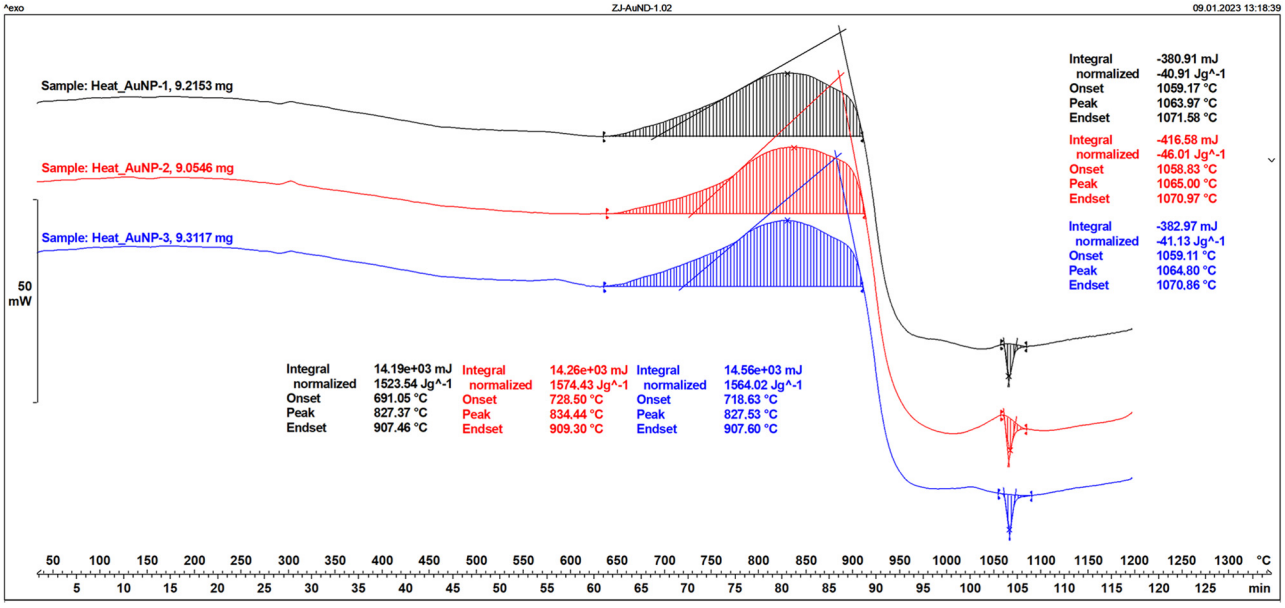


**Figure 10:** DSC curves of the sintering and melting of dried AuNPs.

temperature values of the melting point of various nanomaterials indicates that the proposed method of determining the melting temperature point by indirect methods, such as TEM, nanocalorimetry, and X-ray diffraction, is not entirely adequate. The reason is that, in most cases, the measurements are not carried out under normal conditions. Thus, in TEM, it is considered that the observed nanomaterials are in a high vacuum, and, at the same time, TEM focuses exclusively on individual nanoparticles, and not on a group of nanoparticles, as our sample was a cake of dried AuNPs. The mentioned methods also do not allow the detection of exothermic sintering, as was revealed by DSC analysis.

Based on the results of the DSC analysis, we can conclude that the AuNPs synthesised by the USP method and lyophilisation can be pressed at room temperature with a simple compression method, as there will be no significant change in their melting point. This suggests that such dried AuNPs can be used for thin layer and subsequent low-temperature fusion of the deposited AuNPs into the bulk Au state. It is concluded that this represents a new potential of AuNPs for the preparation of corrosion-resistant and highly conductive materials on flexible and less temperature-resistant materials, such as wood, polymers, and organic tissues.

## 4 Conclusions

The scientific work of determining the melting temperature of AuNPs synthetised through the coupled process of USP and lyophilisation led to the following findings:

- The high-resolution Au 4f XPS spectrum revealed two well-defined Au $4f_{7/2}$ and Au $4f_{5/2}$ core lines. They were additionally deconvoluted into two components. Considering the Au $4f_{7/2}$ band, the measured BE values occur between the BE typically obtained for $Au^0$ (83.8 ÷ 84.0 eV) and $Au^+$ (85.6 eV). This suggests that the initially formed AuNPs do not have the same properties as bulk Au.
- Dried AuNPs have a polycrystalline character, which was confirmed by XRD analysis.
- The uniaxial microcompression triggered room temperature sintering of the AuNPs when the compression stress exceeded 250 MPa.
- DSC analysis revealed that AuNPs undergo exothermic sintering from $T$ = 712°C to $T$ = 908.1°C.
- The melting point of dried AuNPs is about 1064.3°C and is very similar to bulk gold (1064.2°C).
- No phenomenon called melting-point depression was found in the dried AuNPs.

**Funding information:** This research was funded by the Slovenian Research Agency Training and funding of a Young Researcher, (Co) Financing Agreements nos. 1000-19-0552, 1000-20-0552, and 1000-21-0552 and Research Programme P2-0120.

**Author contributions**: All authors have accepted responsibility for the entire content of this article and agree with its submission.

**Conflict of interest**: The authors state no conflict of interest.

## References

[1] Chow PE. Gold nanoparticles: Properties, characterization and fabrication. New York: Nova Science Publishers, Inc; 2010. p. 343.
[2] Dykman LA, Khlebtsov NG. Methods for chemical synthesis of colloidal gold. Russ Chem Rev. 2019;88(3):229–47.
[3] Daruich De Souza C, Ribeiro Nogueira B, Rostelato MECM. Review of the methodologies used in the synthesis gold nanoparticles by chemical reduction. J Alloy Compd. 2019;798:714–40. doi: 10.1016/j.jallcom.2019.05.153.
[4] Zhao P, Li N, Astruc D. State of the art in gold nanoparticle synthesis. Coord Chem Rev. 2013;257(3):638–5.
[5] Brust M, Walker M, Bethell D, Schiffrin DJ, Whyman R. Synthesis of thiol-derivatised gold nanoparticles in a two-phase Liquid–Liquid system. J Chem Soc Chem Commun. 1994;7:801–2.
[6] Daniel MC, Astruc D. Gold nanoparticles: assembly, supramolecular chemistry, quantum-size-related properties, and applications toward biology, catalysis, and nanotechnology. Chem Rev. 2004;104(1):293–346.
[7] Hammami I, Alabdallah NM, Jomaa AAl, Kamoun M. Gold nanoparticles: Synthesis properties and applications. J King Saud Univ - Sci. 2021;33(7):10.
[8] Mehravani B, Ribeiro AI, Zille A. Gold nanoparticles synthesis and antimicrobial effect on fibrous materials. Nanomaterials. 2021;11(5):37.
[9] Majerič P, Rudolf R. Advances in ultrasonic spray pyrolysis processing of noble metal nanoparticles-Review. Materials (Basel). 2020;13(16):28.
[10] Jelen Ž, Majerič P, Zadravec M, Anžel I, Rakuša M, Rudolf R. Study of gold nanoparticles' preparation through ultrasonic spray pyrolysis and lyophilisation for possible use as markers in LFIA tests. Nanotechnol Rev. 2021;10(1):1978–92.
[11] Cortie MB, Van Der Lingen E. Catalytic gold nano-particles. Mater Forum. 2002;26(January 2002):1–14.
[12] Waghmare RB, Perumal AB, Moses JA, Anandharamakrishnan C. Recent developments in freeze drying of foods. Innov Food Process Technol A Compr Rev. 2020;(August):82–99.
[13] Takagi M. Electron-diffraction study of liquid-solid transition of thin metal films. J Phys Soc Jpn. 1954;9(3):359–63.
[14] Wang G, Wu N, Wang J, Shao J, Zhu X, Lu X, et al. Abnormal change of melting points of gold nanoparticles confined between two-layer graphene nanosheets. RSC Adv. 2016;6(110):108343–6.

[15] Qiao Z, Feng H, Zhou J. Molecular dynamics simulations on the melting of gold nanoparticles. Phase Transit. 2014;87(1):59–70. doi: 10.1080/01411594.2013.798410.
[16] Das A, Ghosh MM. MD simulation-based study on the melting and thermal expansion behaviors of nanoparticles under heat load. Comput Mater Sci. 2015;101:88–95. doi: 10.1016/j.commatsci.2015.01.008.
[17] Naffziger S, Beck N, Burd T, Lepak K, Loh GH, Subramony M, et al. Pioneering chiplet technology and design for the AMD EPYC™ and Ryzen™ processor families: Industrial product. Proc - Int Symp Comput Archit, 2021-June; 2021. p. 57–70.
[18] Li T, Hou J, Yan J, Liu R, Yang H, Sun Z. Chiplet heterogeneous integration technology—status and challenges. Electron. 2020;9(4):1–12.
[19] Sun W, Liu JJ, Zhang H. When Smart wearables meet intelligent vehicles: Challenges and future directions. IEEE Wirel Commun. 2017;June:58–65.
[20] John Dian F, Vahidnia R, Rahmati A. Wearables and the Internet of Things (IoT), Applications, opportunities, and challenges: A survey. IEEE Access. 2020;8:69200–11.
[21] Niknejad N, Ismail WB, Mardani A, Liao H, Ghani I. A comprehensive overview of smart wearables: The state of the art literature, recent advances, and future challenges. Eng Appl Artif Intell. 2020;90(February):103529. doi: 10.1016/j.engappai.2020.103529.
[22] Lymberis A. Smart wearables for remote health monitoring, from prevention to rehabilitation: Current RandD, future challenges. Proc IEEE/EMBS Reg 8 Int Conf Inf Technol Appl Biomed ITAB, 2003-Janua; 2003. p. 272–5.
[23] Mainak S. Gupta R, Nguyen TA, editors. Smart multifunctional nano-inks: Fundamentals and emerging applications. Amsterdam, Netherlands: Elsevier; 2022. p. 726.
[24] Jeong BS, Woo K, Kim D, Lim S, Kim JS, Shin H, et al. Controlling the thickness of the surface oxide layer on Cu nanoparticles for the fabrication of conductive structures by ink-jet printing. Adv Funct Mater. 2008;18(5):671–830.
[25] Jiang H, Moon K, Hua F, Wong CP. Thermal properties of tin/silver alloy nanoparticles for low temperature lead-free interconnect technology temperature (OC). 2007 Proceedings 57th Electronic Components and Technology Conference, NV, USA, 2007, pp. 54–8.
[26] Haynes WM. Haynes WM, Lide DR, Bruno TJ, editors. CRC handbook of chemistry and physics. Vol. 21. Boca Ranton: Taylor & Francis; 2020. p. 2643.
[27] Rudolf R, Majerič P, Štager V, Albreht B. Process for the production of gold nanoparticles by modified ultrasonic spray pyrolysis: patent application no. P-202000079. Ljubljana: Office of the Republic of Slovenia for Intellectual Property; Slovenia: Ljubljana: Urad RS za intelektualno lastnino; 2020.
[28] Dzimitrowicz A, Jamroz P, Greda K, Nowak P, Nyk M, Pohl P. The influence of stabilizers on the production of gold nanoparticles by direct current atmospheric pressure glow microdischarge generated in contact with liquid flowing cathode. J Nanopart Res. 2015;17(4):10. doi: 10.1007/s11051-015-2992-7.
[29] Koczkur KM, Mourdikoudis S, Polavarapu L, Skrabalak SE. Polyvinylpyrrolidone (PVP) in nanoparticle synthesis. Dalt Trans. 2015;44(41):17883–905.
[30] Schneider CA, Rasband WS, Eliceiri KW. NIH Image to ImageJ: 25 years of image analysis. Nat Methods. 2012;9(7):671–5. doi: 10.1038/nmeth.2089.
[31] Majerič P, Jenko D, Friedrich B, Rudolf R. Formation mechanisms for gold nanoparticles in a redesigned ultrasonic spray pyrolysis. Adv Powder Technol. 2017;28(3):876–3.
[32] Janecek M, Kral R, editors. Modern electron microscopy in physical and life sciences. IntechOpen; 2016. doi: 10.5772/60494.
[33] Minicò S, Scirè S, Crisafulli C, Galvagno S. Influence of catalyst pretreatments on volatile organic compounds oxidation over gold/iron oxide. Appl Catal B: Environ. 2001;34:277–85.
[34] Sylvestre J, Poulin S, Kabashin AV, Sacher E, Meunier M, Luong JHT, et al. Surface chemistry of gold nanoparticles produced by laser ablation in aqueous media. J Phys Chem B. 2004;108:16864–9.
[35] Casaletto MP, Longo A, Martorana A, Prestianni A, Venezia AM. XPS study of supported gold catalysts: the role of Au 0 and Au + d species as active sites. Surf Interface Anal Int J Devoted Dev Appl Tech Anal Surf Interfaces Thin Films. 2006;38(4):215–8.
[36] Bulushev DA, Yuranov I, Suvorova EI, Buffat PA. Highly dispersed gold on activated carbon fibers for low-temperature CO oxidation. J Catal. 2004;224:8–17.
[37] Muto H, Yamada K, Miyajima K, Mafune F. Estimation of surface oxide on surfactant-free gold nanoparticles laser-ablated in water. J Phys Chem C. 2007;111:17221–6.
[38] Gerthsen D, Nienhaus GU. Nanoscale Facile preparation of water-soluble fluorescent gold nanoclusters for cellular imaging applications†. Nanoscale. 2011;3:2009–14.
[39] Bratescu MA, Cho SP, Takai O, Saito N. Size-controlled gold nanoparticles synthesized in solution plasma. J Phys Chem C. 2011;115:24569–76.
[40] Bjelajac A, Phillipe AM, Guillot J, Fleming Y, Chemin JB, Choquet P, et al. Gold nanoparticles synthesis and immobilization by atmospheric pressure DBD plasma torch method. Nanoscale Adv. 2023;5:2573–82.
[41] Kumar A, Mandal S, Selvakannan PR, Pasricha R, Mandale AB, Sastry M. Investigation into the interaction between surface-bound alkylamines and gold nanoparticles. Langmuir. 2003;19(15):6277–82.
[42] Chen CC, Zhu C, White ER, Chiu CY, Scott MC, Regan BC, et al. Three-dimensional imaging of dislocations in a nanoparticle at atomic resolution. Nature. 2013;496(7443):74–7.
[43] Mayer AE. Micromechanical model of nanoparticle compaction and shock waves in metal powders. Int J Plast. 2021;147(August):103102. doi: 10.1016/j.ijplas.2021.103102.
[44] Rubenis K, Zemjane S, Vecstaudza J, Lazdovica K, Bitenieks J, Wiecinski P, et al. Sintering of amorphous calcium phosphate to near-full density by uniaxial compaction at room temperature. J Eur Ceram Soc. 2022;42(13):6199–205. doi: 10.1016/j.jeurceramsoc.2022.06.041.
[45] Fernández-Pérez A, Rodríguez-Casado V, Valdés-Solís T, Marbán G. Room temperature sintering of polar ZnO nanosheets: II-mechanism. Phys Chem Chem Phys. 2017;19(25):16413–25.
[46] Dai X, Xu W, Zhang T, Shi H, Wang T. Room temperature sintering of Cu-Ag core-shell nanoparticles conductive inks for printed electronics. Chem Eng J. 2019;364(January):310–9. doi: 10.1016/j.cej.2019.01.186.
[47] Wakuda D, Kim KS, Suganuma K. Room temperature sintering of Ag nanoparticles by drying solvent. Scr Mater. 2008;59(6):649–52.
[48] Koga K, Ikeshoji T, Sugawara KI. Size- and temperature-dependent structural transitions in gold nanoparticles. Phys Rev Lett. 2004;92(11):2–5.
[49] Shariq M, Friedrich B, Budic B, Hodnik N, Ruiz-Zepeda F, Majerič P, et al. Successful synthesis of gold nanoparticles through ultrasonic

spray pyrolysis from a Gold(III) nitrate precursor and their interaction with a high electron beam. ChemistryOpen. 2018;7(7):533–42.
[50] Schmid M, Wegener K. Additive manufacturing: polymers applicable for laser sintering (LS). Procedia Eng. 2016;149(June):457–64. doi: 10.1016/j.proeng.2016.06.692.
[51] Dick K, Dhanasekaran T, Zhang Z, Meisel D. Size-dependent melting of silica-encapsulated gold nanoparticles. J Am Chem Soc. 2002;124(10):2312–7.
[52] Mittal J, Lin KL. Exothermic low temperature sintering of Cu nanoparticles. Mater Charact. 2015;109:19–24. doi: 10.1016/j.matchar.2015.09.009.
[53] Averin SI, Alymov MI. Sintering diagrams of gold powders. Inorg Mater Appl Res. 2013;4(5):385–8.
[54] Coutts MJ, Cortie MB, Ford MJ, McDonagh AM. Rapid and controllable sintering of gold nanoparticle inks at room temperature using a chemical agent. J Phys Chem C. 2009;113(4):1325–8.
[55] Wang BX, Zhou LP, Peng XF. Surface and size effects on the specific heat capacity of nanoparticles. Int J Thermophys. 2006;27(1):139–51.
[56] Jeong J, Wang Y. Thermal properties of copper nanoparticles at different sintering stages governed by nanoscale heat transfer. Addit Manuf Lett. 2023;4(December 2022):100114. doi: 10.1016/j.addlet.2022.100114.